Boundary equivalent model and optimization of glass fiber reinforced composite storage tanks based on theory of plates and shells

Journal of Physics: Conference Series **2888** (2024) 012007 doi:10.1088/1742-6596/2888/1/012007

Boundary equivalent model and optimization of glass fiber reinforced composite storage tanks based on theory of plates and shells

Jiangle Song[1], Dong Chen[1,*], Yifan Su[1], Dan Wang[2], Jianwei Shi[1], Kai Cui[1], Wenjie Wang[1], Nao-Aki Noda[3,4,5]

[1] School of Mechanical and Power Engineering, Zhengzhou University, No. 100 Science Avenue, Zhengzhou, 450001, China

[2]School of Chemical Engineering, Zhengzhou University, No. 100 Science Avenue, Zhengzhou, 450001, China

[3]Department of Mechanical and Control Engineering, Kyushu Institute of Technology, Sensui-Cho 1-1, Tobata, Kitakyushu, Fukuoka, Japan

[4]College of Mechanical Engineering, Tianjin University of Science and Technology, Tianjin, 300222, China

[5]Tianjin Key Laboratory of Integrated Design and On-line Monitoring for Light Industry & Food Machinery and Equipment, Tianjin, 300222, China

***** Corresponding author: chen.dong@zzu.edu.cn

Abstract. Glass fiber reinforced composites are widely used in storage tanks for corrosive liquids such as hydrochloric acid. In order to solve the leakage problem of a certain factory's storage tanks. The type and failure region were located through investigation, sampling, and mechanical testing. By considering the specific conditions, a boundary equivalent model was proposed and derived from the theory of plates and shells. It can locate and measure the cause of failure accurately, without complex numerical modelling process. By focusing on the three key parameters that can avoid failure, the tank design was optimized and the bending stress in the failure region was reduced by 43% without changing the production cost and anti-dumping ability.

Keywords: composite material; thin-walled tank; glass fiber; theory of plates and shells

1. Introduction

Glass fiber reinforced polymer (GFRP) composite, are widely used in aerospace, marine industry, automotive, energy storage and other fields in order to take their advantages of light weight, high specific strength, high specific modulus, and strong corrosion resistance [1–4]. In current industry practice, while designed to store corrosive liquids like hydrochloric acid, GFRP was selected for manufacturing large

thin-walled storage tanks through autoclave forming [5–7]. However, due to some outdated design theory in previous design procedure, a large number of leakage and fracture happen among the produced GFRP storage tanks during service. Therefore, it is necessary to check the rationality of the design and correct unreasonable parameters. In addition, as the thickness of the tank is much less than the general size, difficulties such as element distortion and non-convergence arise in the process of finite element method (FEM) analysis [8–12]. Besides, there is also difficulty in shell modelling if the wall thickness is not varying linearly along the structure. Due to these reasons, doing thin-walled tank design by using modern tools such as FEM and other simulation method [13] may require experience and skills for engineering applications [14–23]. Therefore, in this study an equation was derived from Timoshenko's theory of plates and shells [24]. It can be used to calculate bending stress and describe deformation of the specific thin-walled large size tank with middle-area-raised bottom plate (MARBP), conveniently. By observing the actual usage process, MARBP of thin-walled tank will contact with ground after fulfilled with liquid. Based on tank's practical deformation process during service, boundary equivalent model (BEQM) was proposed to simplify the derivation and calculation process. By using the derived equation and proposed BEQM, key parameters that influence the failure intensity have been addressed and optimized.

2. Sample preparation and mechanical testing

As shown in Fig. 1, the research object is a GFRP thin-walled storage tank with a height H_t of $7000mm$ and a diameter of $6000mm$. A large number of damages have occurred during actual service, and it can be measured that the thinnest thickness of the tank is $14mm$, as shown in Fig. 2a. In order to determine the cause of failure, the analysis sample was cut from the bottom plate of the storage tank as shown in Fig. 2. Fig. 2a shows the crack location and schematic diagram of the analysis sample, and Fig. 2b shows the photo of a cut sample, where the thinnest thickness was measured.

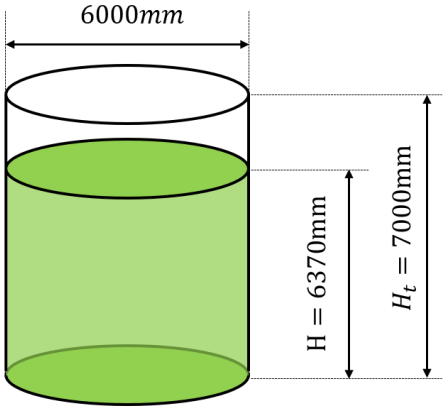

Fig. 1. Diameter and height of the thin-walled tank with MARBP

By observing and analyzing the cut sample, it was confirmed that there are cracks along the junction of the bottom plate where the boundary of raised middle area locates. The cracks propagated thoroughly from the bottom surface of the bottom plate to the upper surface, where the reason of liquid leakage can be addressed.

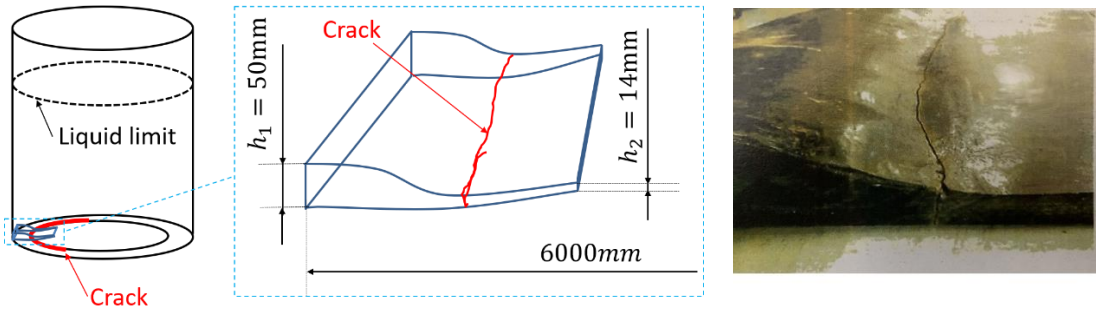

(a) Location of crack where samples were cut off (b) Photo of crack region

Fig. 2. Sample preparation and its photo

For mechanical test, 20 specimens with rectangular cross-section were prepared. The length of the specimen is $250mm$, and they were cut from the intact area [25] of the storage tank. As shown in Fig. 3, by following the JIS-K6911 testing standard for heat hardening plastics, a three-point bending test was conducted to measure the general elastic parameters of the GFRP material. The thickness of the specimen along the load direction is $h = 10mm$, and the width perpendicular to the load direction is $b = 11mm$. The load P is transmitted through a high Cr steel cylinder with a radius of $5mm$, which locates at the midpoint of two supports with a loading speed of $5mm/min$. The supports are cylindrical with a radius of $2mm$, and the distance between the two supports is $l = 160mm$. The bending force P and displacement Δx were recorded by using Changchun Kexin WDW300. Then the macroscopic mechanical parameters Young's modulus E of the tank GFRP can be calculated by using Eq. (1), and as the main basis for subsequent calculations. The failure stress σ_{max} of the material can be calculated by using Eq. (2) from the failure load P_{max}.

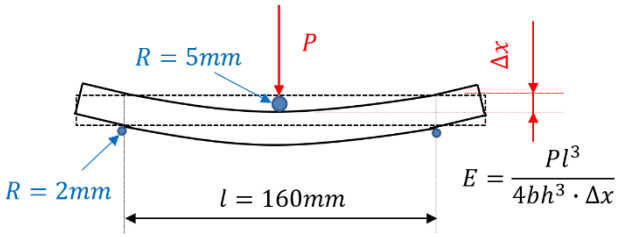

Fig. 3. Schematic of three point bending test

$$E = \frac{Pl^3}{4bh^3 \cdot \Delta x} \tag{1}$$

$$\sigma_{max} = \frac{3P_{max}l}{2bh^2} \tag{2}$$

Table 1. Bending properties of the GFRP

Maximum Load P_{max}	Failure bending stress σ_{max}	Young's modulus E
$688.8N$	$116MPa$	$6900MPa$

Least squares curve fitting method was used to obtain the bending Young's modulus from 20 repeat tests. While for maximum load when fracture happen P_{max}, the minimum value in the record was selected.

3. MARBP shell model and its deformation

Create a section along the rotation center of the storage tank, forming a side view of the tank as shown in Fig. 4. The blue color represents the shape of the tank when it is not loaded with liquid, and red color represents the shape of the area where the MARBP shape undergoes significant changes when it is filled with liquid. When viewed from the top of the tank, the suspended MARBP of empty tank is a circular area. During the liquid loading process, liquid pressure causes downward bending deformation from the center, the center first contacts the ground, then the contact area gradually expands.

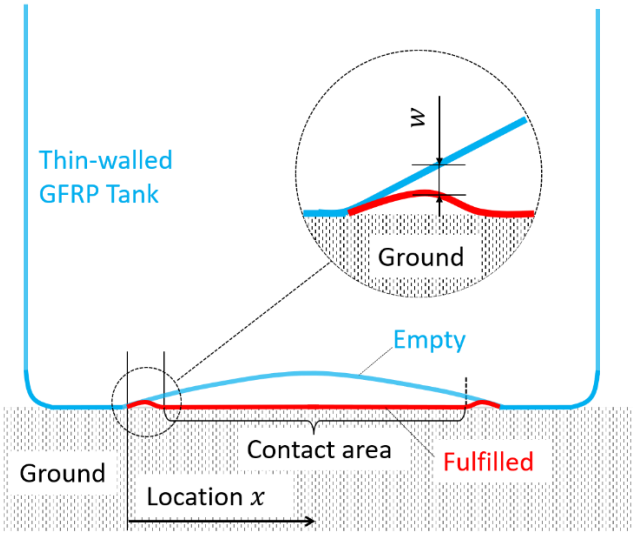

Fig. 4. Comparison of empty and fulfilled tank

4. BEQM modelling

The stiffness of ground is concrete, which is much higher compared with bottom plate, therefore the shape of the bottom plate has almost no further deformation after contact with the ground. The upper surface is subjected to liquid pressure, and the lower surface is supported by the ground. As shown in Fig. 5, the contact area can be simplified as a circular plate with curved boundaries and compressed on both sides. For thin-walled GFRP storage tanks, bending deformation is the main form, so the thickness change caused by compression on both sides can be ignored. Therefore, the contact area can be assumed as a rigid body. Establish a cylindrical coordinate system, where $r = 0$ represents the center position and $r = a$ represents the maximum radius of the MARBP, which is the boundary between the suspended area and the ground support area. The edge of the contact area between the bottom plate of the loaded liquid and the ground are denoted by $r = b$.

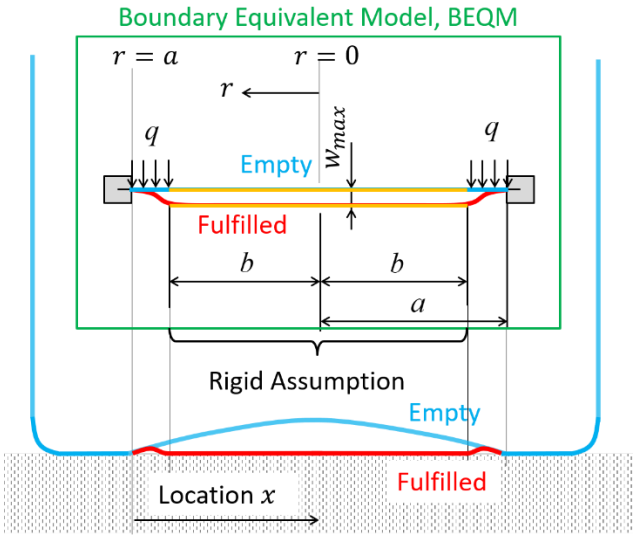

Fig. 5. BEQM where MARBP touches ground

For the BEQM in Fig. 5, the following boundary conditions as shown in Eq. (3) should be met.

$$\begin{cases} \left(\frac{dw}{dr}\right)\Big|_{r=b} = 0 \\ \left(\frac{dw}{dr}\right)\Big|_{r=a} = 0 \\ w|_{r=b} = w_{max} \\ w|_{r=a} = 0 \end{cases} \tag{3}$$

The uniformly distributed pressure on a rigid circular plate is represented by q, and Q represents the shear force of the outer structure that supports the inner region at the boundary whose radius is r. Pressure q in the ground contacted zone can be regarded offset, as it no longer contributes to deformation in $b \le r \le a$ area. Therefore, equilibrium Eq. (4) exists for the remain suspended zone $b \le r \le a$.

$$2\pi rQ = \pi(r^2 - b^2)q \tag{4}$$

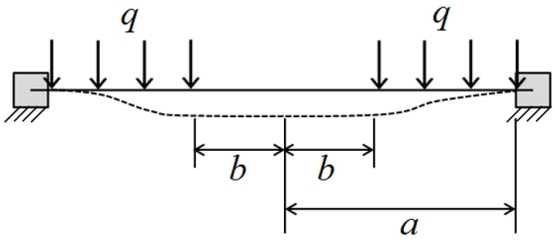

Fig. 6. BEQM model with rigid assumption

As shown in Fig. 6, the tank model is simplified as a rigid body in the middle region $r < b$, a plate shell model in the circular region $b < r < a$ subjected to uniformly distributed load q, and a fixed constraint at $r = a$. According to Eq. (4), the supporting shear force Q can be obtained from Eq. (5):

$$Q = \frac{r^2 - b^2}{2r} q = \frac{qr}{2} - \frac{qb^2}{2} \frac{1}{r} \tag{5}$$

According to Timoshenko's shell theory[24], there are equations (6) and (7):

$$D = \frac{Eh^3}{12(1 - v^2)} \tag{6}$$

$$\frac{d}{dr}\left[\frac{1}{r}\frac{d}{dr}(r\frac{dw}{dr})\right] = \frac{Q}{D} \tag{7}$$

Substitute Eq. (5) into Eq. (7) and integrate r on both sides of the equation to obtain Eq. (8). The solution for the constant maturity term C_1 generated by integration can be found in Eq. (11).

In current analysis, the contacting deformation process of the MARBP after loading liquid, i.e. $r > 0$ is mainly focused. Therefore, Eq. (8) is simplified and integrated again to obtain Eq. (9), where $\ln(x)$ represents the logarithmic operation based on the natural number e, i.e. $\log_e(x)$.

$$\frac{1}{r}\frac{d}{dr}(r\frac{dw}{dr}) = \frac{qr^2}{4D} + C_1 - \frac{qb^2}{2D}\ln r \tag{8}$$

$$\frac{dw}{dr} = \frac{qr^3}{16D} + \frac{C_1 r}{2} + \frac{C_2}{r} - \frac{qb^2}{2D}\left[\frac{1}{2}r\ln r - \frac{1}{4}r\right] \tag{9}$$

Integrate Eq. (9) on r can get Eq. (10):

$$w = \frac{qr^4}{64D} + \frac{C_1 r^2}{4} + C_2 \ln r + C_3 - \frac{qb^2}{8D} r^2 \ln r + \frac{qb^2}{8D} r^2 \tag{10}$$

Combine Eq. (3), (8) and (9) can get：

$$\begin{aligned} C_1 &= \frac{-q(a^2 + b^2)}{8D} + \frac{qb^2[b^2(2\ln b - 1) - a^2(2\ln a - 1)]}{4D(b^2 - a^2)} \\ C_2 &= \frac{qa^2b^2}{16D} + \frac{qb^4\{-a^2[2\ln a - 1] + a^2[2\ln b - 1]\}}{8D(a^2 - b^2)} \\ C_3 &= -\frac{qa^4}{64D} - \frac{a^2}{4}C_1 - C_2 \ln a + \frac{qa^2b^2}{8D}\ln a - \frac{qa^2b^2}{8D} \end{aligned} \tag{11}$$

5. Numerical calculation and parameter optimization

So far, only two variables remain unknown, that is radius b where MARBP contacts with ground after loaded liquid and vertical displacement of MARBP from empty shape to the fulfilled. If the two variables are known, the maximum bending stress at any position in the remain-suspended area can be calculated using Eq. (12), where h represents the thickness of the structure [24]. According to the rigid assumption

of the suspended area mentioned above, the vertical displacement w at full load is the maximum possible value of w at the contact boundary $r = b$, that is, the height w_{max} of the suspended structure from the ground when unloaded at position $r = b$, as shown in Fig. 5.

$$M_r = -D\left(\frac{d^2w}{dr^2} + \frac{v}{r}\frac{dw}{dr}\right)$$
$$(\sigma_r)_{max} = -\frac{6M_r}{h^2} \tag{12}$$

According to the coordinate system shown in Fig. 5, the height of the MARBP from the ground at position x is represented by $h_s(x)$, which can be obtained by measuring the specific geometric dimensions of the empty suspended area of the tank body. When the assumed area size of the rigid body is b, the vertical displacement of the equivalent model rigid body area in Fig. 6 is represented by $w|_{r=b}$. For different b values, $w|_{r=b}$ can be obtained by Eq. (10) and (11) respectively, i.e. $w|_{r=b}$ is a function of b. It is easy to know that if $h_s(x)$ equals $w|_{r=b}$, the shape curves of the remaining suspended area of the two models completely overlap when fulfilled with liquid. Therefore, the size of b can be determined by solving Eq. (13). In order to more intuitively demonstrate the solving process, the curves of two variables changing with x are shown in Fig. 7, and the final solution of b, is from the intersection point of the two curves.

$$h_s(x) = w|_{r=b} \tag{13}$$

According to specific engineering requirement, it can be seen that the maximum depth of the liquid is $6370mm$, and the liquid density is $\rho = 1.14\,g/cm^3$, MARBP radius is $a = 2600mm$, GFRP elastic modulus is shown in Table 1. By using the proposed calculated method, the radius of the contact area is $400mm$, and the bending stress distribution is shown in Fig. 8. The maximum bending stress is $106.6MPa$, which is less than 8.2% of the material failure limit shown in Table 1. It no longer met the design requirements of relevant safety factors of actual service conditions, where the bending stress at this location is a pulse cycle from 0 to the maximum value. Therefore, fatigue failure ultimately leads to crack propagation [26,27] and liquid leakage.

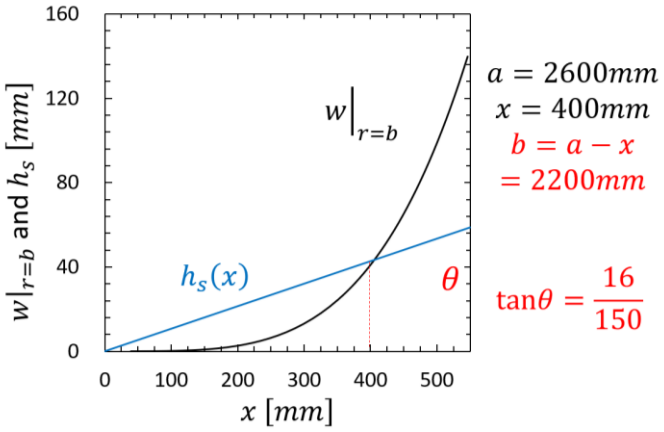

Fig. 7 Calculating the radius b of contact zone

Based on the equation derived above, the optimize determination is to reduce the bending stress in

the failure area. It can be seen that an effective method is to reduce $\tan\theta$ the slope of $h_s(x)$, increase the thickness h or reduce the radius a of the MARBP. Increasing h will significantly increase the manufacturing cost of the storage tank, while reducing a will affect the tank's resistance to tipping hazards caused by deformation. Therefore, adjust $\tan\theta$ is the best choice. By adjusting from 16/150 to 10/150, the radius of MARBP contact area is reduced from 400 to 350 when filled with liquid, and the maximum bending stress is reduced from 106.6 MPa to 60.0 MPa.

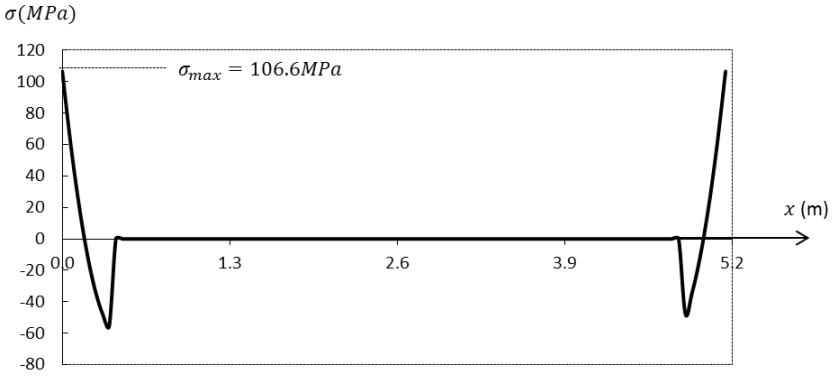

Fig. 8. MARBP bending stress distribution of fulfilled tank

6. Conclusion

In order to address the inappropriate design in glass fiber reinforced polymer (GFRP) composite thin-walled large size storage tanks that met leakage fracture during service life, this paper addresses its failure type and region through investigation, sampling, and mechanical test. By considering the specific conditions and derived from the theory of plates and shells, proposed a boundary equivalent model (BEQM). Finally, the tank parameters were optimized to reduce bending stress. The following conclusions have been reached:

(1) Through investigation and sampling of failed large-sized GFRP liquid storage tanks, the causes and failure modes of leakage were determined. Mechanical properties of GFRP during service after autoclave forming were measured and determined.

(2) By introducing rigid body assumption based on shell theory, BEQM was proposed. It is suitable for thin-walled structures of rotating bodies with middle area raised bottom plate (MARBP) that suspended under no load and contact with the ground when filled with liquid. Theoretical derivation and numerical calculations were carried out to determine the key area that consistent with the actual failure location. By calculating the bending stress, the accuracy of the proposed model was also verified.

(3) Taking advantage of the monotonicity of the derived function, three key parameters $\tan\theta$, a and h that influence quality of design were quickly determined. The parameter $\tan\theta$ with least economic and safety costs were selected for optimization, and the bending stress in the original failure area was reduced by 43% with rarely changing the production cost and anti tipping ability of the original product.

Acknowledgements

This study was supported by National Natural Science Foundation of China (Grant Numbers: 12302106, 22206174, 52305292, 52175153). The authors also appreciate the financial support from National

Natural Science Foundation of Henan (Grant No. 232300421321), Postdoctoral Fellowship Program of CPSF (Grant No. GZC20232394) and Key Research & Development and Promotion Project of Henan Province (Grant No. 242102220117).

References

[1] Malfroy J, Van Bavel B, Steelant J and Vandepitte D 2024 Thin-walled tapered conformable low-pressure tanks: Concept and principles *Thin-Walled Struct.* **197**

[2] Han J-S, Yoon J-C and Lee H 2024 Analysis of Deposition Characteristics of Thin-Wall Structures using the Directed Energy Deposition Process *Trans. Korean Inst. Electr. Eng.* **73** 631–6

[3] Wang X, Chen X, Yang J, Xie P and Yang W 2023 Research on torsional laminated extrusion for improving the permeability and mechanical properties of HDPE/PA6 composite for type IV storage tank liners *J. Appl. Polym. Sci.* **140**

[4] Farahmandpey S, Broumand P, Mehrab Amiri S and Reza Shekari M 2023 On the nonlinear dynamic analysis of annular baffled steel containers isolated by bearings *Structures* **56**

[5] Wang D, Fang H, Xue R and Li S 2024 Numerical study on the axial collapse of thin-walled columns *Sci. Rep.* **14**

[6] Zhang Y, Liu Z, Xin J, Wang Y, Zhang C and Zhang Y 2021 The attenuation mechanism of CFRP repaired corroded marine pipelines based on experiments and FEM *Thin-Walled Struct.* **169**

[7] Zhang Y, Guo Z, Zhao H, Ma G and Zhang F 2021 Analysis of torsional instability and reliability of marine flexible pipelines *Ocean Eng.* **228**

[8] Chen D, Zhang G W, Takaki R, Inoue A, Tsuboi K, Sano Y and Noda N-A 2018 Intensity of singular stress fields of an embedded fibre under pull-out force *IOP Conference Series: Materials Science and Engineering* vol 369 p 012003

[9] Hu K, Zheng Y, Zhu J, Shi Q, Duan L and Han W 2024 Assessment of tensile damage mechanism of open-hole GLARE laminates based on acoustic emission and digital image correlation techniques *Polym. Compos.* **45** 4788–809

[10] Zheng Y, Hu K, Zhang M, Zhu J, Zhao F, Han W, Shi Q and Cao Z 2024 Characterizing damage patterns and evolution in Multi-Hole GLARE laminates under tensile load via integrated AE and DIC techniques *Compos. Struct.* **331**

[11] Cui K, Song G, Wang W, Liu H, Yang Y, Sun C, Zhao Z, Lin H and Chen D 2024 Force analysis and distribution evolution of Fe3O4 nanoparticles in magnetic fluids *Chinese J. Phys.* **88** 982–90

[12] Noda N-A, Chen X, Sano Y, Wahab M A, Maruyama H, Fujisawa R and Takase Y 2016 Effect of pitch difference between the bolt-nut connections upon the anti-loosening performance and fatigue life *Mater. Des.* **96** 476–89

[13] Qin T Y, Yu Y S and Noda N A 2007 Finite-part integral and boundary element method to solve three-dimensional crack problems in piezoelectric materials *Int. J. Solids Struct.* **44** 4770–83

[14] Wang Z, Noda N-A, Ueno M and Sano Y 2017 Optimum Design of Ceramic Spray Coating Evaluated in Terms of Intensity of Singular Stress Field *Steel Res. Int.* **88**

[15] Li R, Noda N-A, Takaki R, Sano Y, Takase Y and Miyazaki T 2018 Most suitable evaluation method for adhesive strength to minimize bend effect in lap joints in terms of the intensity of singular stress field *Int. J. Adhes. Adhes.* **86** 45–58

[16] Galvez P, Noda N-A, Takaki R, Sano Y, Miyazaki T, Abenojar J and Martínez M A 2019 Intensity of singular stress field (ISSF) variation as a function of the Young's modulus in single lap adhesive joints *Int. J. Adhes. Adhes.* **95** 102418

[17] Chen D, Noda N-A, Takaki R and Sano Y 2020 Intensity of singular stress fields (ISSFs) in micro-bond test in comparison with ISSFs in pull-out test *Int. J. Mech. Sci.* **183** 105817

[18] Noda N-A, Chen D, Zhang G and Sano Y 2020 Single-fiber pull-out analysis comparing the intensities of singular stress fields (ISSFs) at fiber end/entry points *Int. J. Mech. Sci.* **165** 105196

[19] Noda N-A, Chen D and Sano Y 2022 Reference solution and proportional method to calculate intensity of singular stress field (ISSF) at the interface corner where reinforced fiber enters resin matrix *Mech. Adv. Mater. Struct.* **29** 2962–72

[20] Zhu W, Chen D, Shi J, Zhang J, Zhao H and Li C 2024 Design and optimization of a temperature controller with low overshoot, fast respond and high COP based on water-source thermoelectric heat pump *Appl. Therm. Eng.* **242** 122473

[21] Galvez P, Lopez de Armentia S, Abenojar J and Martinez M A 2020 Effect of moisture and temperature on thermal and mechanical properties of structural polyurethane adhesive joints *Compos. Struct.* **247**

[22] Takaki R, Noda N-A, Sano Y, Takase Y, Suzuki Y and Chao C 2021 Fractographic Identification of Fracture Origin Mainly Controlled by the Intensity of Singular Stress Field (ISSF) in Prismatic Butt Joint with Corner Fillet *Int. J. Adhes. Adhes.* **106** 102810

[23] Liu X, Wang B, Noda N-A, Sano Y, Inui Y, Tateishi K and Takase Y 2021 Bolt clamping force versus torque relation (F-T relation) during tightening and untightening the nut having slight pitch difference *Mech. Based Des. Struct. Mach.*

[24] Timoshenko S P and Woinowsky-krieger S 1959 THEORY OF PLATES AND SHELLS

[25] Yin Z, Tie Y, Duan Y, Li C and Chen D 2022 Impact damage assessment in patch-repaired carbon fiber-reinforced polymer laminates using the nonlinear Lamb wave-mixing technique *Polym. Compos.* **in press**

[26] Zhao C, Ren R, Wei Y, Yang G, He B, Zhang K and Zhong J 2022 Crack Propagation for Glass Fiber Reinforced Laminates Containing Flame Retardant: Based on Single-Edge Tensile Loading *Mater. Plast.* **59** 88–99

[27] Zhao C, Ren R, Zhong J, Goh K L, Zhang K, Zhang Z and Le G 2022 Intralaminar crack propagation of glass fiber reinforced composite laminate *Structures* **41** 787–803